Special issue article

SURFACE and INTERFACE ANALYSIS

Received: 1 April 2017 Revised: 14 August 2017 Accepted: 15 August 2017 Published online in Wiley Online Library: 15 September 2017

(wileyonlinelibrary.com) DOI 10.1002/sia.6296

Self-assembled monolayers of octadecylphosphonic acid and polymer films: Surface chemistry and chemical structures studied by time-of-flight secondary ion mass spectrometry

Heng-Yong Nie[a,b]*

With the ever-decreasing thickness of functional organic thin films, surface sensitive analytical techniques are required to probe surface/interface chemistry and structural changes of ultra-thin organic films such as self-assembled monolayers (SAMs) of amphiphilic molecules and polymeric coatings. Time-of-flight secondary ion mass spectrometry (TOF-SIMS) fits this requirement because it is extremely surface sensitive and provides rich chemical information. In this article prepared for celebrating the 35th anniversary of our lab as a surface analysis service provider and a surface science research center, we highlight our TOF-SIMS studies on exploring the surface chemistry of SAMs of octadecylphosphonic acid. Due to our contribution to developing the fast growth method of delivering octadecylphosphonic acid SAMs via the use of solvents having a dielectric constant of 3 to 5, we will review the formation mechanisms of SAMs. We will also review our recent results that demonstrated the feasibility of using the ion intensity ratio between C_6H^- and C_4H^- to differentiate the chemical structures of several polymers and depth profiling the cross-linking degree of a polymer. In this article, we show results from principal component analysis on numerous C_nH^- intensity data from multiple spectra obtained from polyethylene, polypropylene, polyisoprene, and polystyrene. This multivariate analysis method allowed us to better understand the relationships between the polymers and between C_nH^-, as well as verify the rationale for the selection of C_4H^- as the reference ion for normalization. We demonstrate that together with principal component analysis, TOF-SIMS is unique in differentiating chemical structures of polymers. Copyright © 2017 John Wiley & Sons, Ltd.

Keywords: octadecylphosphonic acid self-assembled monolayers; surface chemistry; TOF-SIMS; ion intensity ratio; chemical structures of polymers; principal component analysis

Introduction

Surface often plays a vital role in governing the functionalities of a material related to its surface chemistry or electronic properties. Therefore, control of the surface of materials is imperative to developing applications that rely on their surface-related functionalities. For example, self-assembled monolayers (SAMs) of amphiphilic organic molecules formed on a solid substrate have aroused enormous interest in interdisciplinary areas such as molecular engineering of surfaces, tribology, biology, nanotechnology, composite polymers, organic electronics, and analytical chemistry.[1,2] In this particular surface modification using surfactants, it basically makes use of a high-energy surface as the substrate to anchor amphiphilic molecules, from which functionalities can be incorporated via the terminal groups of the molecules. Casting thin polymer films on a substrate is another approach to achieve a functionalized surface for applications in photoresists, antibacterial surfaces and biological sensors.[3,4] More recently, development of organic semiconductors has led to a new industry of organic electronics, where functional polymer films including semiconductors and dielectrics are usually solution-processed on a substrate.[5,6]

To ensure the chemical stability of SAMs, it is important to determine the selectivity of organic molecules used to modify a particular substrate. On the other hand, to achieve appropriate chemical stability and mechanical strength for solution-processed polymer films, their molecules need to be cross-linked.[7–10] With the ever-decreasing thickness of functional organic thin films used in organic electronic devices and nanotechnology,[11–13] required are analytical approaches that are surface sensitive enough to probe surface/interface chemistry and structural changes through the thickness of ultra thin organic films. Time-of-flight secondary ion mass spectrometry (TOF-SIMS)[14] perfectly fits this requirement because it is extremely surface sensitive.[15–18] In this technique, a

* Correspondence to: Heng-Yong Nie, Surface Science Western, The University of Western Ontario, London, Ontario, N6G 0J3, Canada.
E-mail: hnie@uwo.ca

a Surface Science Western, The University of Western Ontario, London, Ontario, N6G 0J3, Canada

b Department of Physics and Astronomy, University of Western Ontario, London, Ontario, N6A 3K7, Canada

pulsed (primary) ion beam (eg, Bi_3^+) is used to bombard the surface of a specimen to generate (secondary) ions from the topmost monolayer (1-3 nm), whose mass and intensity are registered as an ion mass spectrum. With a sputter ion beam (eg, C_{60}^+)[19,20] to remove a controllable amount of substance, TOF-SIMS is also capable of depth profiling the specimen with nanometer-scale resolutions.[21,22]

However, TOF-SIMS is not a quantitative technique because ion yields (the fraction of the sputtered atoms or molecules that become ions) can be significantly different for different atoms or molecules and may vary depending on their chemical environment.[23,24] This matrix effect often complicates the interpretation of TOF-SIMS results of organic material, which is a research theme towards development of semiquantitative analysis approaches.[25] Nevertheless, TOF-SIMS has proven a powerful exploratory tool for understanding chemical structures of organic films and surface chemistry of SAMs. For example, although many ions fragmented from octadecylphosphonic acid (OPA) SAMs do not directly render chemical interactions between the organic molecules and the substrate, certain ions bear information about the chemical states of the molecules interacting with the substrate.[18] For polymers, the patterns of ion fragmentation and/or the intensity ratios of certain ions are useful in revealing their chemical structures.[26,27] In other words, there are ions that have intrinsic relationships, whose intensity ratios cancel the factors determining their measured intensities and are thus capable of revealing their relationships with the chemical structures of polymers.

The rich chemical information provided by TOF-SIMS ion mass spectra lies in the form of fragment ions, which often amount to hundreds, leading to the possibility of identifying chemicals and exploring surface chemistry. Facing such a daunting number of ions (ie, variables) detected in TOF-SIMS, dimensionality reduction techniques such as principal component analysis (PCA), a multivariate data analysis method,[28,29] have proven useful in revealing similarities or differences of ions in terms of the variability of their intensities and can be used to differentiate a polymer with different molecular weights or different polymers.[30–34] The original variables (ie, ions in the TOF-SIMS case) are transformed to a much smaller number of new orthogonal variables (ie, PCs), which are linear combinations of the original variables. The PCs are transformed from the original data under the condition that the first PC accounts for as much of the variance in the original data as possible, with the following PCs picking up the remaining maximum variances subsequently.[28] Principal component analysis allows one to compare numerous observations (data) over multiple variables in a biplot, which is constructed by a plot of the scores of the observations on 2 PCs (often the first 2 PCs) overlapped with a plot of loadings of the variables on the same 2 PCs.[35] A biplot visualizes the similarities and differences among the observations, their relationships with the variables, and the correlations between the variables.

In this article, we review the research results on our exploring formation mechanisms of OPA SAMs and their surface chemistry studied with TOF-SIMS.[36–46] Surface modification using OPA SAMs has indeed seen a wide variety of applications in controlling surface properties of metal oxides.[47–55] Our results in preparing and characterizing OPA SAMs have proven useful in further understanding the surface chemistry of this SAM system and promoting its applications.[18,39,51,56,57] We also review our more recent results associated with the development of TOF-SIMS analytical approaches to differentiating the chemical structures of polyethylene (PE), polypropylene (PP), polyisoprene (PIP), and polystyrene (PS), as well as quantifying cross-linking degrees and depths of poly(methyl methacrylate) (PMMA) using the intensity ratio between hydrocarbon ions C_6H^- and C_4H^-, denoted as ρ.[26,27] We found that ρ increases with increased "carbon density," which is largely related to the C/H ratio.[26] To understand relationships among more hydrocarbon ions C_nH^-, we present in this article PCA of these hydrocarbon ions to investigate relationships among C_nH^- intensities for PE, PP, PIP, and PS for the purpose of answering the question as why ρ is a measure of "carbon density". An ION-TOF GmbH (Münster, Germany) TOF-SIMS IV has been used in our laboratory since 1999. The TOF-SIMS data presented in our publications reviewed in this article were obtained using either a 9 keV $^{133}Cs^+$ beam[18,40,45] or a 25 keV Bi_3^+ beam[26,27,46] as the primary ion beam.

With the review of relevant past work and new results on PCA of C_nH^- intensities for the 4 polymers, this article is expected to stimulate further effort towards development of analytical approaches for exploring surface chemistry of OPA SAMs and identifying chemical structures of polymers using the powerful TOF-SIMS technique.

Formation mechanisms of OPA SAMs

There are 2 approaches to form ordered molecular monolayers on a solid surface: Langmuir-Blodgett (LB) film and the conventional SAMs. In the LB approach, an external force is applied to compress the amphiphilic molecules spread on a liquid subphase to form a crystalline (Langmuir) monolayer on the subphase (eg, water) surface.[58] Such a Langmuir monolayer transferred to a substrate emerged from (or inserted to) the subphase becomes an LB film. Repeating this process renders multilayer LB films on the substrate. On the other hand, the conventional SAM approach is to immerse a substrate in a solution of amphiphilic molecule so that the molecules are adsorbed on the substrate.[59–62] This approach requires that the molecules have a strong interaction with the substrate so that they can be anchored to the substrate covalently and eventually form closely packed monolayer via van der Waals forces between the molecular chains. Thus, this method requires a good match between the molecule and substrate; for example, the most studied 2 SAM systems are (1) alkanethiols on coinage metals with an S-metal bond formation[59,60] and (2) organosilanes on oxides where condensation and polymerization of silanols are responsible for the monolayer formation.[61,62] For the past 3 decades, there have been a wide variety of applications in engineering surface with SAMs.[1,63,64] While SAMs have been investigated for more than 4 decades, their formation mechanisms are not necessarily well understood, as evidenced by conflicting data presented in the literature.[63]

More recently, OPA has been shown to serve as a more general model system for investigating the fundamentals of SAM formation,[18,39,46,63,65–70] because experimental findings clarified that there are different speciation[18] for OPA headgroups on different substrates. For example, organophosphonic acid is bonded to an oxidized aluminum surface through P–O–Al via condensation reaction of the acidic hydroxyl groups from the molecules with the hydroxyl groups on the oxide surface.[70–72] On the other hand, it was verified that OPA SAMs formed on silicon oxide were anchored by hydrogen bonding, prone to attacks from polar solvents including water.[18,39] These weakly bound SAMs can only be achieved with the new method where a nonpolar solvent having a dielectric constant of 3 to 5 is used to drive the polar headgroups to the medium surface.[39] It is worth noting

SURFACE and INTERFACE ANALYSIS

that weakly bonded OPA SAMs have found an application in metal-dielectric patterning as a resist layer on a Cu-patterned-SiO_2 surface. Upon rinse the OPA molecules were removed from only the SiO_2 surface allowing the deposition of ZnO via the atomic layer deposition technique, while the OPA SAMs modified Cu surface blocked the growth of ZnO.[57]

The traditional SAM formation methods usually require longtime immersion (eg, overnight), which makes such methods challenging for situations where either a spin coating process or dip coating process is preferred for quick turnaround and mass production. For example, in solution process–based organic electronics, spin coating is one of the standard approaches to deposit layers.[12,73,74] The approach of spin coating SAMs would be compatible with the cost saving, high throughput requirement of organic electronics, which is a major driving force for the development of organic electronics in the first place.

Dielectric constant of solvent is a measure of its ability to separate or solvate charged particles. For SAM formation, polar solvents are usually used under the consideration that they dissolve the molecules well. We have demonstrated the concept of using appropriate nonpolar solvents with a dielectric constant of 3 to 5 as an active medium to concentrate and align the polar headgroups of amphiphilic molecules on its surface so that the molecules are in a state to seek hydrophilic entities. This presents a new SAM formation approach, which facilitates fast growth of SAMs, enabling spin coating and dip coating suitable for industrial scale production. This method has been shown to result in applications in depositing SAMs on the dielectric surface in organic thin-film transistors.[51–55] The only requirement in this method is physical contact between the medium and the substrate, allowing fast growth of SAMs on any hydrophilic substrate via spin coating[18,39,43,51,54,55] and dip coating.[46] Although metals or metal oxides are inherently hydrophilic, in practice, surface cleaning is needed because of the presence of adventitious hydrocarbons on the surface of almost any substrate exposed to air for a certain period. Common methods include UV/ozone and plasma treatment, as well as etching. Since cleaved mica substrate provides a clean and atomically flat surface, it is an ideal substrate to verify the coverage of OPA SAMs when atomic force microscopy (AFM) is used to image the OPA SAMs. For example, in our early stage of investigating OPA SAMs, we noticed the impact of humidity on the morphology of SAMs spin coated on a hydrophilic substrate. Under low-humidity conditions, the substrate is covered by a layer with small pores while under high-humidity conditions, island-like monolayers without pores. However, adding more OPA solution to the existing monolayers will eventually fill out the pores or gapes for the 2 cases, respectively.

Dielectric constant of solvent has been identified as the key player in producing such a "high potential energy" medium observed experimentally.[39] We have confirmed that nonpolar solvents such as trichloroethylene (3.4), anisole (4.3), and chloroform (4.8) work. By contrast, polar solvents such as ethanol (24.6), dichloromethane (9.1), and trichloroethane (7.5), as well as nonpolar solvent with too small a dielectric constant, such as toluene (2.4), dodecane (2.0), heptane (1.9), and hexane (1.9), do not work.

The explanation for this method is, as depicted in Figure 1A, that the interaction between the OPA molecules and the solvent molecules renders a situation where the OPA polar headgroups align on the medium surface, only when the solvent has a dielectric constant in the range of 3 to 5. These aligned molecules will be spontaneously transferred onto a hydrophilic surface upon their physical contact to form a monolayer. If a substrate (or an object) with a hydrophilic surface is inserted into such a medium, OPA

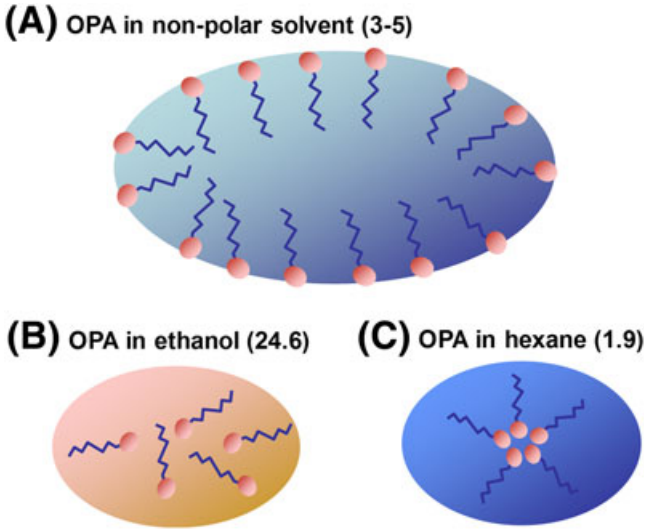

Figure 1. Illustration of octadecylphosphonic acid (OPA) molecules, with the waved line representing the hydrocarbon chain and the filled circle the headgroup, dissolved in (A) nonpolar solvents with a dielectric constant in the range of 3 to 5, (B) a polar solvent, such as ethanol (with a dielectric constant of 24.6), and (C) a nonpolar solvent, such as hexane (1.9). Only solvents with a dielectric constant of 3 to 5, such as trichloroethylene (3.4), chloroform (4.8), and anisole (4.3) render the OPA polar headgroups concentrated on medium surface. The illustration (A) is reproduced from H.-Y. Nie, N.S. McIntyre, and W.M. Lau. Selective removal of OPA molecules from their self-assembled monolayers formed on a Si substrate, J. Phys: Conf. Ser. 61, 869-873 (2007), with the permission of IOP Publishing.

headgroups will be driven to the newly formed interface between the medium and the substrate. Therefore, either spin coating or dip coating works equally well for delivering OPA SAMs on the hydrophilic surface.[39,46] By contrast, for a polar solvent (eg, ethanol) and a nonpolar solvent having a very low dielectric constant (eg, hexane), OPA molecules disperse well (Figure 1B) and form inverted micelles (Figure 1C) in the medium, respectively.

TOF-SIMS analyses of OPA SAMs

The TOF-SIMS, due to its surface sensitivity, has proven powerful in exploring organic molecular monolayer systems including alkanethiols, fatty acids, and organophosphonic acids,[75–81] whose thickness is on an order of 2 nm. Therefore, TOF-SIMS probes both the hydrocarbon chains of the molecules in the SAMs and the interactions between their headgroups and the substrate, which is either a metal or metal oxide. Ions generated from SAMs may carry information about chemical structures of the molecule and interfacial chemistry determined by the interaction between the headgroup and the substrate. Alkane thiol monolayers and multilayers have been used as a model system for TOF-SIMS to investigate ion yields of atomic and cluster ions associated with the molecules and the gold substrate as a function of number of layers.[76] Thiol SAMs prepared on a gold substrate were found to degenerate in air as evidenced by detection of alkanesulfonate ions, which was dependent on the length of the hydrocarbon chain.[77,78] The TOF-SIMS investigations on OPA SAMs on tantalum oxide, with the help of some other analytical techniques, revealed the bonding configuration of the molecular headgroups and the substrate.[79] In a comparison study conducted on alkanethiol and OPA SAMs using several analytical techniques including TOF-SIMS,

OPA was confirmed to form ordered monolayers on oxides.[80] By correlating the intensities of PO_2^- or PO_3^- from OPA SAMs formed on a mica substrate against cosine of its water contact angle, it was found that TOF-SIMS can be used to infer wettability of OPA-modified surfaces.[81]

The chemical stability of SAMs on a substrate is determined by the strength of the interaction between the molecular headgroups and the substrate. As described above, OPA SAMs can be delivered on both Al and Si oxides with 2 distinctive configurations of headgroup-substrate interaction: The molecules are covalently bonded to Al oxide but attached to Si oxide via hydrogen-bonding. These 2 model systems allow us to use TOF-SIMS to explore the interfacial chemistry of OAP SAMs. It was found that TOF-SIMS can readily differentiate the 2 OPA SAMs systems.[18]

Shown in Figure 2 are secondary negative ion mass spectra in m/z 62 to 84 obtained (using a 25 keV Bi_3^+ primary ion beam) on OPA SAMs prepared on Al and Si oxides. The most significant difference between the 2 spectra is that the OPA SAMs on Si oxide have a much more abundant PO_3H^- than their counterpart on Al oxide. By contrast, both have similarly abundant PO_3^-. Since the OPA molecules in their SAMs on Si oxide are attached to the surface via hydrogen-bonding, the 2 hydroxyl groups are intact. Therefore, PO_3H^- is the deprotonated headgroup of OPA. For OPA SAMs on Al oxide, because of the linkages of P–O–Al formed via condensation reaction, PO_3H^- is weak and can be tentatively attributed to the combination of PO_3^- and a hydrogen atom in space above the sample surface where both are abundant. Therefore, the bonding modes between the OPA headgroup and the substrate are readily captured by ion intensity ratios between certain characteristic ions associated with the headgroup. For example, the intensity ratio of PO_3H^- against PO_3^- for OPA SAMs on Al oxide was 0.05, while it became 0.54 on Si oxide. It is thus clear that fragmentation of acids is different from their salts, which is useful for one to use TOF-SIMS to explore interfacial chemistry of OPA SAMs.

As described above, TOF-SIMS readily differentiates covalently bonded OPA headgroups on Al oxide from those via hydrogen-bonding on a Si oxide. However, we have not yet figured out as what are the TOF-SIMS criteria for differentiating whether the covalent bonding is mono-, di- or tridentate (shown in the upper panel of Figure 2 is a bidentate bonding scenario). There are some other techniques that may be used to differentiate different bonding states. For example, Fourier-transform infrared spectroscopy has been used to look at the presence (or absence) of absorption peaks of P–OH and P=O.[82,83] There is a report on oxidizing gold surface as a way to render different bonding modes of organophosphonic acids on its surface.[82] Therefore, it is worth mentioning that if the 3 bonding modes can be realized, TOF-SIMS criteria, perhaps by way of relationships among the intensity ratios of ions including at least PO_2^-, PO_3^-, and PO_3H^-, may be discovered.

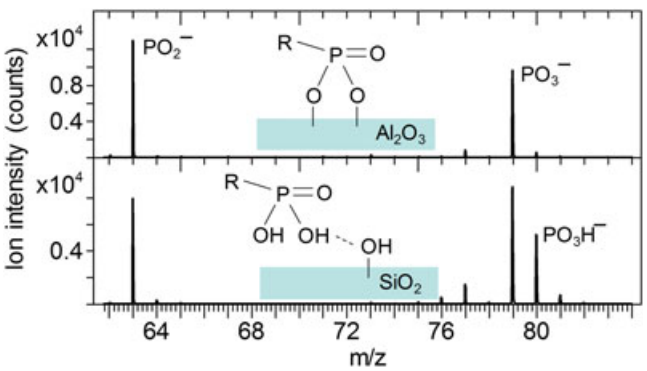

Figure 2. Secondary negative ion mass spectra of octadecylphosphonic acid (OPA) self-assembled monolayers on Al and Si oxides. The bonding modes of OPA molecules with the 2 different substrates are also depicted.

For OPA SAMs on Si oxide, the positive and negative ions for the condensed dimer of OPA molecules $C_{36}H_{77}P_2O_5^+$ (651) and $C_{36}H_{75}P_2O_5^-$ (649), corresponding to $[M-OH_2+H]^+$ and $[M-OH_2-H]^-$, respectively, are detected, where M = $C_{18}H_{39}PO_3$ is the molecular formula of OPA.[18] These 2 ions of the OPA condensed dimer are also seen from OPA powder. However, these 2 ions are absent from OPA SAMs on Al oxide, suggesting that the OPA molecules in their SAMs have to be "free" to generate these dimer ions under the TOF-SIMS primary ion bombardment. It is clear from our TOF-SIMS results that whether the headgroup of an OPA molecule is attached to the headgroup of another OPA molecule or an oxide via hydrogen-bonding, its chemical identity remains the same.

We also applied TOF-SIMS to study kinetics of oxidation of the alkyl chains of molecules in OPA SAMs on Si oxide caused by UV/ozone exposure.[45] When exposed to UV/ozone for 5 minutes, the intensity of the OPA molecular ion $C_{18}H_{38}PO_3^-$ reduced to 27% of that of the original, suggesting an oxidation of the hydrocarbon chains, also evidenced by abundant CH_3O^-, C_2HO^-, CHO_2^-, and $C_4H_5O_2^-$. While CH_3O^- is a relatively abundant ion from ethylene glycol, C_2HO^- is a rather ubiquitous ion for anything that contains carbon, hydrogen, and oxygen. The detection of CHO_2^- and $C_4H_5O_2^-$ usually indicates the presence of carboxylates and methacrylate, respectively. The oxidation characterized by the detection of the ions from those functional groups with high surface energy is responsible for surface energy enhancement, which is the reason UV/ozone treatment[84] is used to improve the wettability of polyesters for print and adhesion applications. However, AFM imaging confirmed that there were no morphological changes detected at this stage. Based on those TOF-SIMS and AFM results, we thus concluded that oxidation of molecular chains precedes the disruption of the molecular structural integrity. This is the grounds for patterning using SAMs as a template via localized surface oxidation.

We have developed a dip coating process for forming OPA SAMs on Al films using anisole, an environment-friendly solvent selected solely by its dielectric constant[39] being 4.3 and investigated their thermal stability.[46] The Al films were dipped into the solution for only a couple of seconds, rendering OPA SAMs formed on the surface of the substrates. The TOF-SIMS analyses on OPA SAMs heated to 150°C in air showed that the intensity of the OPA molecular ion $C_{18}H_{38}PO_3^-$ remained and the static water contact angles were still as high as approximately 120°, demonstrating the excellent thermal stability of OPA SAMs on Al films.[46] We confirmed that oxidation of the hydrocarbon chains occurred when temperatures were raised to 200°C, as evidenced by increased abundance of C_2HO^- and CO_2H^-. Since the annealing experiment was performed in air, the abundance of CN^- and CNO^- was also observed to increase significantly upon annealing at 300°C and beyond.

TOF-SIMS analyses of polymers

For polymers, either a positive or negative ion mass spectrum has hundreds of ions, from which selected ions must be identified to make use of the rich chemical information provided by TOF-SIMS. For any organic material, carbon cluster and hydrocarbon ions are ubiquitous. Making use of these ubiquitous ions to explore the

chemical structure of polymers has been pursued since the early stage of TOF-SIMS. For example, Briggs pointed out that the intensity ratio between C^- and CH_2^- is higher for unsaturated hydrocarbons than saturated ones.[85,86] For example, the intensity ratio for PE and PS is 1.1 and 5.8, respectively.[86] The surface chemical structures of various polymers have been successfully characterized using intensity ratios between selected ions.[87] Positive hydrocarbon ions $C_xH_y^+$, with their intensities normalized to that of $C_2H_3^+$, have been found to have different values for different polyolefins, such as polyethylene and polypropylene.[88] Ligot et al reported a study on correlating the mechanical properties with cross-linking degrees of ethyl lactate-based plasma polymer films synthesized by plasma-enhanced chemical vapor deposition.[33] The cross-linking degrees, determined by plasma power, were presented by the average chemical composition of the hydrocarbon ions. For example, it was determined that the calculated average hydrocarbon "ions" for polymer films made at plasma power of 30 and 280 W were $C_{6.5}H_{6.6}$ and $C_{4.8}H_{4.1}$, respectively. These averaged "ions" rendered C/H ratios of 0.98 and 1.17, respectively, which corresponded to hardness of 0.51 and 0.74 GPa as determined by nanoindentation.[33]

As evidenced by the TOF-SIMS applications reviewed above, ion intensity ratios, rather than ion intensities themselves, are more useful in revealing chemical structures of polymers. This is because intensities of individual ions are a function of many variables such as measuring conditions and the chemical environment––they are hardly a quantitative measure of the chemical structure of the specimen. If there are ions that are fragmented from the same chemical structure, then their intensity ratios will likely cancel the factors determining their actual intensities and thus reveal their relationships with the chemical structures of the specimen. This is indeed a process of removing uncertainties and trying to quantitatively assess some aspects of the chemical structure, which are otherwise lost in the ample amounts of ions. Rather than treating each ion as a stand-alone attribute, we believe that certain ions must possess intrinsic relationships, which can be used to understand the chemical structures of polymers. It is thus important to identify ions that serve to reveal the chemical structure of the specimen in question, which will lead to development of analytical approaches to explore the surface chemistry of materials.

Based on this line of reasoning, we have developed a TOF-SIMS approach to looking at chemical structures of polymers in terms of measuring their "carbon density" via the intensity of C_6H^- normalized to that of C_4H^-, denoted as $\rho = [C_6H^-]/[C_4H^-]$. We have found that ρ provides a measure for "carbon density" defined as the number of carbon atoms bonded to a carbon atom in the hydrocarbon chains of polymers.[26] It is worth pointing out that although C_6H^- and C_4H^- are ubiquitous in TOF-SIMS for any hydrocarbon-containing substance, we have verified that their intensity ratios appear to quantify "carbon density" of polymers. We also confirmed that the other 2 larger hydrocarbon ions C_8H^- and $C_{10}H^-$ also work, except for the fact that their intensities are weaker than that of C_6H^-.

The chemical structures of PE (monomer: C_2H_4), PP (C_3H_6), PIP (C_5H_8), PMMA ($C_5O_2H_8$), and PS (C_8H_8) and measured ρ values are illustrated in Figure 3. As reported in 2 previous publications,[26,27] their ρ values are 20%, 23%, 27%, 32%, and 53%, respectively. These values were estimated from the ion intensities collected using a 25 keV Bi_3^+ primary ion beam. If other primary ion beams were used, the actual values would change. For example, when using a 25 keV Bi^+, Bi_3^{2+}, or Bi_5^+ primary ion beam, PE showed a ρ value of 5%, 18%, or 27%, respectively.[26]

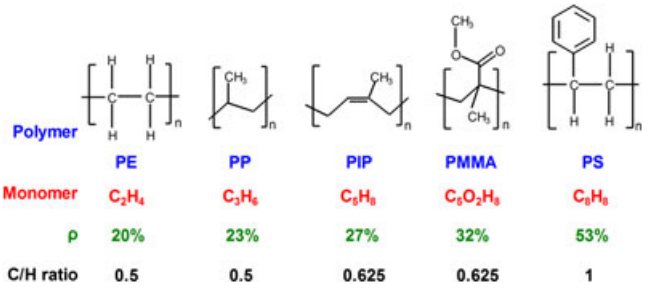

Figure 3. The chemical structures, ρ values, and C/H ratios of polyethylene (PE), polypropylene (PP), polyisoprene (PIP), poly(methyl methacrylate), and polystyrene (PS). The ρ values were estimated from ion intensities of C_6H^- and C_4H^- from ion mass spectra obtained using a 25 keV Bi_3^+ primary ion beam. The portion of PE, PP, PIP, and PS in this figure is adopted from H.-Y. Nie, J. Vac. Sci. Technol. B 2016, 34, 030603, with the permission of the American Vacuum Society.

Among the 5 polymers, PE has the smallest and PS the largest ρ. This correlates to the fact that PE and PS have the smallest and largest "carbon density," respectively. For PE, every carbon atom is linked to 2 carbon atoms in the hydrocarbon chain, while for PS, there are double bonds from benzene ring. It is interesting to note that although both PE and PP have the same C/H ratio of 0.5, ρ is larger for PP (23%) than for PE (20%). From the chemical structures of PE and PP shown in Figure 3, there is a carbon atom that is bonded to 3 carbon atoms in PP, while in PE, each carbon atom is bonded to 2 carbon atoms. Therefore, the "carbon density" of PP is larger than that of PE. This is also the reason that we choose to use "carbon density," rather than C/H ratio to describe ρ. Another interesting observation is that PMMA and PIP have a ρ of 32% and 27%, respectively, although their C/H ratios are the same (ie, 0.625). For these 2 polymers, we are not sure whether this difference in ρ is due to (1) the presence of oxygen in PMMA or (2) the fact that there is a carbon atom in PMMA that is bonded to 4 carbon atoms, while in PIP there is a carbon atom that is bonded to 3 carbon atoms. For PS, with a C/H ratio of 1, its ρ is 53%, the highest among the 5 polymers. Therefore, it appears that ρ increases with increased C/H ratios. However, for polymers with the same C/H ratio, we apparently need to look at the "carbon density," that is, the carbon atom that is bonded to as many carbon atoms as possible (up to 4).

We also demonstrated that ρ is suitable to gauge the cross-linking degree of PMMA films that were spin-coated on a Si wafer and cross-linked using the hyperthermal hydrogen induced cross-linking (HHIC)[89] technology.[27] The bombardment of energetic H_2 projectiles on the surface of a polymer film results in cleavage of C–H of hydrocarbon chains, generating carbon radicals leading to formation of C–C bond between adjacent hydrocarbon chains.[89] Because HHIC is a surface sensitive cross-linking technology, depth profiling the cross-linking degrees on a nanometer scale requires a surface sensitive analytical technique. The uniqueness of TOF-SIMS lies in its ability to depth-profile with a sputter ion beam (a 10 keV C_{60}^+ion beam in our case) to remove controllable amounts of substance without significantly degrading the remaining surface.[20–22]

At the surface of the PMMA films, ρ for the control is 32%, while for the 10-, 100-, and 500-second HHIC-treated PMMA films, it increases to 45%, 56%, and 65%, respectively.[27] The depth profiles of PMMA characteristic ions, such as $C_4H_5O_2^-$ and $C_8H_{13}O_2^-$, serve to verify the cross-linking of PMMA and confirm the recovery of the PMMA ions after the cross-linked portion is removed by C_{60}^+ sputtering. The depth profiling of ρ revealed that ρ decreases

exponentially, from which depths of cross-linking were estimated. The depth of cross-linking for PMMA films cross-linked upon the HHIC treatment for 10, 100, and 500 seconds was 3, 15, and 40 nm, respectively.[27] Our TOF-SIMS results demonstrated that ρ is suitable to serve as a criterion leading to the quantification of both the degree and depth of cross-linking. This TOF-SIMS approach is considered unique in assessing cross-linking degrees of ultra thin films where use of existing techniques is perhaps not practical.[3,4,8–10]

PCA of C_nH^- intensities for PE, PP, PIP, and PS

Our TOF-SIMS studies on several polymers confirmed that each of them has a specific ρ and ρ increases with increased "carbon densities."[26] We also found that for cross-linked PMMA films, ρ increased with increased cross-linking degrees.[27] These experimental observations suggest that C_6H^- and C_4H^- have an intrinsic relationship, and their intensity ratio is perhaps a measure of "carbon density." The selection of C_4H^- as the reference to scale the intensity of C_6H^- (as well as C_8H^- and $C_{10}H^-$) is based on an observation that the intensity of C_4H^- showed the "lowest" degree of variability for PE, PP, PIP, and PS in comparison with that of CH^-, C_2H^-, C_6H^-, C_8H^- and $C_{10}H^-$. That is, for lower "carbon density" polymer such as PE and PP, CH^- and C_2H^- are abundant with weak C_6H^-, C_8H^-, and $C_{10}H^-$, while for higher "carbon density" polymers such as PS, the intensities of C_6H^-, C_8H^-, and $C_{10}H^-$ increase with decreased abundance of CH^- and C_2H^-. To explore the underlying mechanisms as why the ion intensity of $C_{2n}H^-$ relative to that of C_4H^- provide so much useful chemical information, we compare ion intensities of hydrocarbon ions C_nH^- (n = 1 to 10) for the 4 polymers. This is indeed a problem associated with multivariables (ie, C_nH^-) for various observations (ie, ion intensities of C_nH^- obtained from different polymers). We thus rely on PCA, a multivariate analysis method, to investigate the relationship of C_4H^- with other C_nH^-.

Ion intensities of hydrocarbon ions C_nH^- from 8 to 11 spectra obtained using a 25 keV Bi_3^+ ion beam from 2 samples for each of the 4 polymers PE, PP, PIP, and PS are used to perform PCA. The 39 observations (ie, the ion intensities measured on the 4 polymer samples) are normalized by the total ion intensity and by C_4H^- intensity, for which we have 10 variables (ie, C_nH^- with n = 1 to 10) and 9 (C_nH^-/C_4H^-, excluding n = 4), respectively. For the convenience of discussing PCA and the TOF-SIMS results, variables and C_nH^-, as well as observations and ion intensities, are used interchangeably. We first prepare a table of 39 rows and 10 columns for the ion intensity data normalized by total ion intensity, where each column contains the intensities of a C_nH^- for the 39 spectra and each row corresponds to the ion intensities of the 10 C_nH^- from an area of a polymer sample. The data are shown in Table 1, which is used to generate a 39 × 10 matrix.

The *prcomp()* function of the open source R[90] programming language for statistical computing was used to perform PCA via the singular value decomposition of a data set (such as the one shown in Table 1) **X** as follows. $\mathbf{X} = \mathbf{USV}^T$ where in our case, **X** is the 39 × 10 data matrix, **U** the left singular matrix (39 × 10), **S** a diagonal matrix (10 × 10) containing ordered singular values, and **V** the right singular matrix (10 × 10). **X** is scaled as $\boldsymbol{X}/\sqrt{n-1}$, with *n* being the number of the rows (39 in our case), so that the singular values equal to the square roots of the eigenvalues of PCs. The *prcomp()* function returns the standard deviations (ie, square roots of eigenvalues) from **S**, PC scores of observations (each column of **US** present scores of all observations on each PC**)** and PC loadings of variables (each column of **V** presents loadings of all variable on each PC). Principal component analysis is done after the original data in each C_nH^- column in Table 1 are centered and standardized, which gives a unit variance for the data in each and every column. This scaling ensures that both the abundant and weak ions are treated via their variabilities, rather than their abundances.

Shown in Figure 4A is the scree plot of variances (ie, eigenvalues) of all the 10 PCs resulted from PCA of the data normalized to total ion intensity. Also, shown in the figure are cumulative percentages of variances explained by all PCs. Because ion intensities for each variable (ie, each C_nH^-) are scaled to have a unit variance, the total variance of the data set with 10 variables (C_nH^-, n = 1 to 10) is 10. As shown in Figure 4A, the variances explained by PC1 and PC2 are 5.92 and 2.79, or 59.2% and 27.9% of the total variance, respectively. Together, the first 2 PCs explain 87.1% of the total variance.

The loadings of C_nH^- on the first 2 PCs are shown in Figure 4B, which construct the eigenvectors defining the axes of the PCs transformed from the original data. The loading of a variable on a PC is the weighted contribution of the variable to the PC. As shown in Figure 4B, the loadings of C_6H^- to $C_{10}H^-$ on PC1 are quite similar and the largest, meaning that they are the major contributors to PC1. Those of C_2H^- and C_3H^- on PC1 are similar, too, but with an opposite sign. The 3 most significant contributors to PC2 are C_2H^-, C_3H^-, and C_4H^-.

Shown in Figure 5 is a covariance biplot plotted with the *ggbiplot()*[91] function used in the *ggplot2* package of R, showing the scores of the 39 observations as points and loadings of the 10 variables as arrowed lines, both on PC1 and PC2, as well as the correlation circle.

The score of an observation on a PC is the sum of the individual ion intensity of each variable multiplied by the loading of the corresponding variable on the PC. In other words, it is the projection of all the C_nH^- intensities of an observation on a PC, or how an observation is expressed as a single point on the PC axis. A score plot is used to determine similarities or differences among observations. The score plot in Figure 5 shows that the 4 polymers are separated into 4 groups, to which their 68% data ellipses are drawn to provide a visual guide for the distribution of their scores.

The loading plot[35] shown in Figure 5 is composed of the loadings of the 10 variables, which are depicted by arrowed lines plotted from the origin to each pair of loadings (on PC1 and PC2) multiplied by their corresponding square roots of eigenvalues. An arrowed line of a variable may be called a "variable vector," serving to point the direction of the variable in the PCs coordinates. The smaller an angle between 2 variable vectors of 2 C_nH^-, the more similarly the 2 variables behave in terms of their variability in their ion intensities. In other words, 2 variables are positively or negatively correlated if the angle between their variable vectors is close to 0° or 180°, respectively. On the other hand, an angle close to 90° indicates that the 2 variables are not correlated at all. The loading plot in Figure 5 shows clearly the similarities among C_6H^- to $C_{10}H^-$ for their significant contributions to PC1. By contrast, the variable vectors of C_2H^- and C_3H^- point to (approximately) the opposite direction and with increased loadings on PC2. This indicates that the intensities of the 2 groups of ions vary in opposite directions, that is, when the ion intensities of one group measured on a polymer sample increase, those of the other group decrease.

Also, shown in the biplot is the correlation circle. The lengths of the variable vectors are also scaled along with the radius of the correlation circle. A variable vector of a C_nH^- with its length close to the

Table 1. Ion intensities of C_nH^- for polyethylene, polypropylene, polyisoprene, and polystyrene normalized by total ion intensity. Columns and rows present variables and observations, respectively. Note that the data are neither centered nor standardized

	CH^-	C_2H^-	C_3H^-	C_4H^-	C_5H^-	C_6H^-	C_7H^-	C_8H^-	C_9H^-	$C_{10}H^-$
PE1	0.11963	0.32777	0.01940	0.06974	0.00600	0.01312	0.00127	0.00241	0.00030	0.00038
PE2	0.11613	0.30857	0.01770	0.06447	0.00564	0.01238	0.00121	0.00239	0.00029	0.00036
PE3	0.11838	0.34129	0.01978	0.07145	0.00605	0.01354	0.00122	0.00246	0.00031	0.00037
PE4	0.12197	0.36309	0.02131	0.07648	0.00661	0.01437	0.00138	0.00260	0.00036	0.00036
PE5	0.12096	0.37774	0.02223	0.07951	0.00684	0.01530	0.00141	0.00276	0.00035	0.00038
PE6	0.13069	0.42238	0.02445	0.08632	0.00742	0.01653	0.00150	0.00275	0.00033	0.00047
PE7	0.11717	0.34839	0.02023	0.07455	0.00638	0.01519	0.00153	0.00290	0.00039	0.00050
PE8	0.10820	0.30584	0.01788	0.06499	0.00569	0.01332	0.00131	0.00252	0.00033	0.00041
PE9	0.13769	0.36224	0.02054	0.07218	0.00614	0.01402	0.00136	0.00249	0.00033	0.00039
PE10	0.14849	0.38320	0.02177	0.07531	0.00642	0.01493	0.00140	0.00263	0.00031	0.00041
PE11	0.14294	0.39292	0.02207	0.07708	0.00662	0.01508	0.00149	0.00265	0.00032	0.00037
PP1	0.19265	0.38741	0.02571	0.09013	0.00844	0.02129	0.00241	0.00449	0.00065	0.00086
PP2	0.17181	0.37180	0.02435	0.08572	0.00804	0.02014	0.00226	0.00426	0.00061	0.00076
PP3	0.18318	0.36406	0.02397	0.08355	0.00793	0.01975	0.00232	0.00435	0.00062	0.00083
PP4	0.19284	0.38267	0.02483	0.08509	0.00803	0.01993	0.00236	0.00449	0.00066	0.00084
PP5	0.18145	0.35082	0.02462	0.08596	0.00818	0.02009	0.00239	0.00426	0.00064	0.00078
PP6	0.17684	0.37354	0.02373	0.08561	0.00800	0.02011	0.00219	0.00423	0.00063	0.00084
PP7	0.09776	0.19834	0.01301	0.04557	0.00439	0.01131	0.00139	0.00214	0.00033	0.00044
PP8	0.10414	0.19963	0.01296	0.04465	0.00419	0.01117	0.00111	0.00213	0.00039	0.00041
PP9	0.10718	0.23095	0.01513	0.05277	0.00480	0.01262	0.00130	0.00248	0.00033	0.00043
PP10	0.10311	0.21091	0.01379	0.04874	0.00465	0.01177	0.00126	0.00230	0.00031	0.00045
PP11	0.09608	0.19263	0.01278	0.04338	0.00419	0.01101	0.00122	0.00219	0.00027	0.00041
PIP1	0.07594	0.25711	0.01656	0.09296	0.00872	0.02530	0.00275	0.00637	0.00085	0.00135
PIP2	0.08007	0.26246	0.01684	0.09342	0.00860	0.02575	0.00284	0.00675	0.00094	0.00138
PIP3	0.08078	0.26160	0.01695	0.09292	0.00870	0.02550	0.00287	0.00652	0.00095	0.00143
PIP4	0.08015	0.25697	0.01652	0.09371	0.00864	0.02512	0.00293	0.00659	0.00095	0.00137
PIP5	0.08002	0.25659	0.01653	0.09419	0.00883	0.02546	0.00288	0.00681	0.00098	0.00139
PIP6	0.10004	0.31848	0.02098	0.11970	0.01097	0.03287	0.00356	0.00842	0.00116	0.00184
PIP7	0.11471	0.32408	0.02086	0.11386	0.01059	0.03122	0.00335	0.00809	0.00116	0.00176
PIP8	0.10725	0.34248	0.02216	0.12400	0.01170	0.03404	0.00397	0.00887	0.00126	0.00197
PS1	0.11738	0.18571	0.01271	0.07128	0.00876	0.03873	0.00540	0.01907	0.00354	0.00834
PS2	0.11888	0.19685	0.01282	0.06951	0.00833	0.03749	0.00500	0.01798	0.00331	0.00711
PS3	0.12691	0.20826	0.01322	0.07349	0.00880	0.03958	0.00541	0.01882	0.00359	0.00807
PS4	0.13124	0.20658	0.01370	0.07740	0.00939	0.04242	0.00574	0.02085	0.00393	0.00883
PS5	0.13404	0.26136	0.01430	0.08501	0.00919	0.04449	0.00550	0.02049	0.00328	0.00816
PS6	0.13237	0.25714	0.01401	0.08216	0.00901	0.04304	0.00540	0.02004	0.00319	0.00779
PS7	0.13313	0.25001	0.01359	0.07858	0.00877	0.04177	0.00523	0.01967	0.00328	0.00790
PS8	0.13815	0.27255	0.01502	0.08911	0.00978	0.04800	0.00589	0.02207	0.00379	0.00937
PS9	0.13781	0.24471	0.01413	0.07848	0.00841	0.04083	0.00511	0.01925	0.00315	0.00771

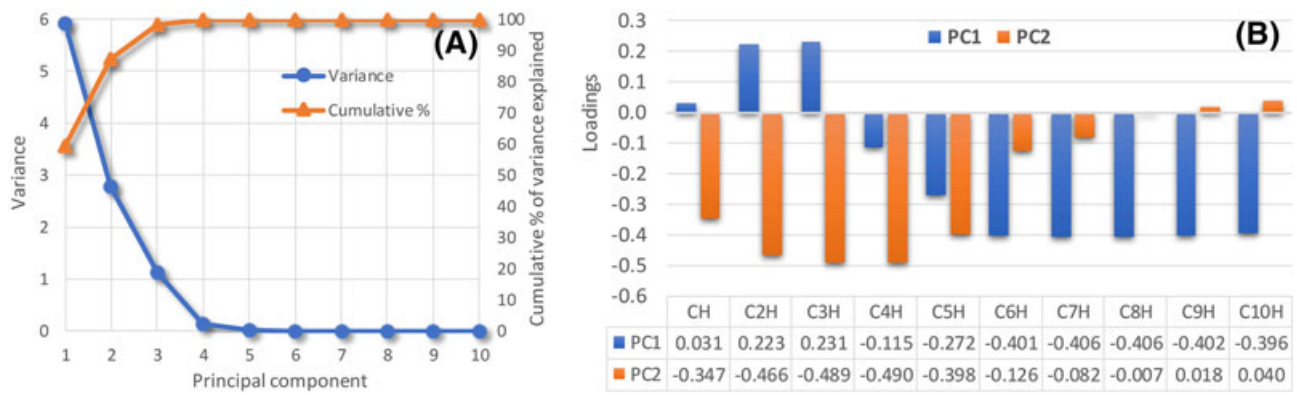

Figure 4. Scree plot of variances of principal components (PCs) and cumulative percentage of variances explained by PCs (A), as well as loadings of the variables (C_nH^-) on PC1 and PC2 (B) for data normalized by total ion intensity.

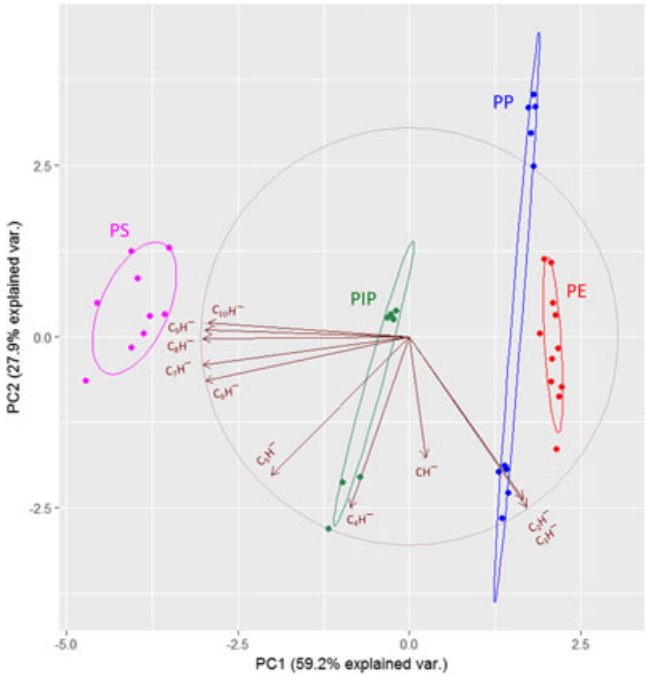

Figure 5. Biplot of scores (points) of observations and loadings (arrowed lines) of variables on PC1 and PC2 from the data normalized by total ion intensity. The 68% data ellipse are shown for scores grouped according to the 4 polymers of polyethylene (PE), polypropylene (PP), polyisoprene (PIP), and polystyrene (PS). Also shown is the correlation circle. The loadings of C_nH^- on each of the 2 PCs are multiplied by the square roots of their corresponding eigenvalues and scaled along with the radius of the correlation circle. PC, principal component.

correlation circle indicates that the variable is well explained by the 2 PCs. If a C_nH^- has a length of its variable vector much shorter than the radius of the correlation circle, it is a sign that the variable is not adequately explained by the 2 PCs. Figure 5, for instance, shows that C_3H^-, C_6H^-, and C_7H^- are explained extremely well by the first 2 PCs, while not so for CH^-.

The beauty of biplot[35,92,93] lies in its ability to visualize the relationships among the numerous observations over multiple variables in score and loading plots overlapped in the landscape of PC1 and PC2. Also, revealed by a biplot are the relationships between the variable vectors and the scores. The projection of a score of an observation to a variable vector is related to the datum of the observation over the original variable. For example, the biplot in Figure 5 shows that scores of PS are largely determined by loadings of C_6H^- to $C_{10}H^-$, while those of PE and PP are positioned on the other side of these loading, with major contributions from loadings of C_2H^- and C_3H^-. It is interesting to note that the scores of PIP are close to the origin of PC1, implying that they are not affected as much either by C_2H^- and C_3H^- or C_5H^- to $C_{10}H^-$.

The PCA results shown in Figure 5 verified our argument that with increased "carbon density," ion intensities of larger C_nH^- increase while those of smaller C_nH^- decrease.[26,27] This is the reason why, over the PC1 axis, PE and PP have their scores on the opposite side of those of PS. It is intriguing to note in Figure 5 that the variable vector of CH_4^- is almost perpendicular to the PC1 axis. This is a reflection that the contribution of CH_4^- to PC1 is minimal, while rather significant to PC2. This suggests that the variability in CH_4^- intensities is the least among other C_nH^- for the 4 polymers. We argue that C_4H^- lies in the middle in terms of the C_nH^- size so that it would have the least variability for different polymers among C_nH^-. This explains our rationale to adopt ρ for gauging the "carbon density" of PE, PP, PIP, and PS.

To further gain insights in understanding the relationships between C_4H^- and other C_nH^-, we repeat PCA with the data normalized by C_4H^- intensity, instead of the total ion intensity. The data set now contains 9 variables (C_nH^-/C_4H^-, excluding n = 4). The C_4H^- column has been removed because it contains a value of 1 in each row, which leads to a zero variance and is not allowed in PCA. The variances explained by all PCs are plotted in Figure 6A with the cumulative percentages of variances explained by all 9 PCs. PC1 and PC2 each explains 7.05 and 1.73 or 78.3% and 19.2% of the total variance of 9, respectively, which are much larger than the percentages their total-ion-intensity-normalized counterparts explain. Together, the first 2 PCs explain 97.5% of the total variance. It is also clear that the variance explained by PC1 has a significant increase in comparison with the case where the ion intensities are normalized by total ion intensity, that is, 78.3% vs 59.2%. On the other hand, PC2 in the case of C_4H^- intensity normalization is smaller than its counterpart in the total ion intensity case, 19.2% vs 27.9%. This suggests that the normalization by C_4H^- presents a better model for PCA than the one by total ion intensity.

As shown in Figure 6B, the 6 major and approximately equal contributors to PC1 are C_5H^- to $C_{10}H^-$. The contributions from C_2H^- and C_3H^- to PC1 are slightly less than C_5H^- to $C_{10}H$, but in an opposite manor. C_1H^- has the least contribution to PC1, but the largest contribution to PC2. The other 2 major contributors to PC2 are C_2H^- and C_3H^-.

Figure 7 shows the biplot for the PCA results obtained from the data normalized by C_4H^- intensity. The striking change is that the deviation in scores on PC2 for PE, PP, and PIP reduces significantly

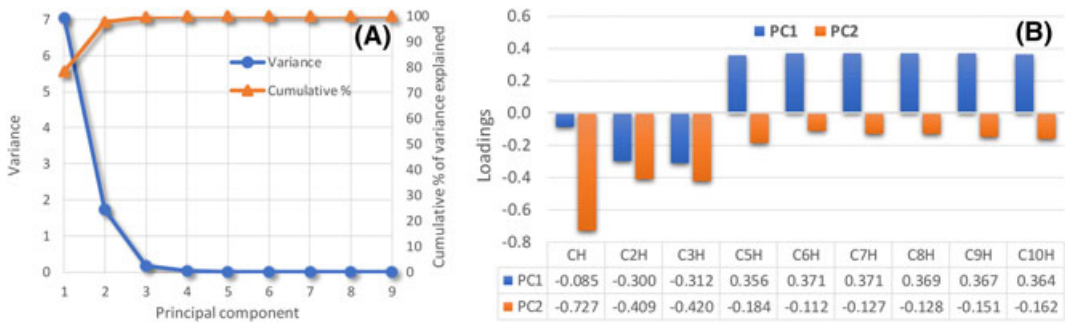

Figure 6. (A) Scree plot of variances of principal components (PCs) and cumulative percentage of variances explained by PCs (B) and loadings of the variables (C_nH^-, excluding C_4H^-) on PC1 and PC2 for data normalized by C_4H^-.

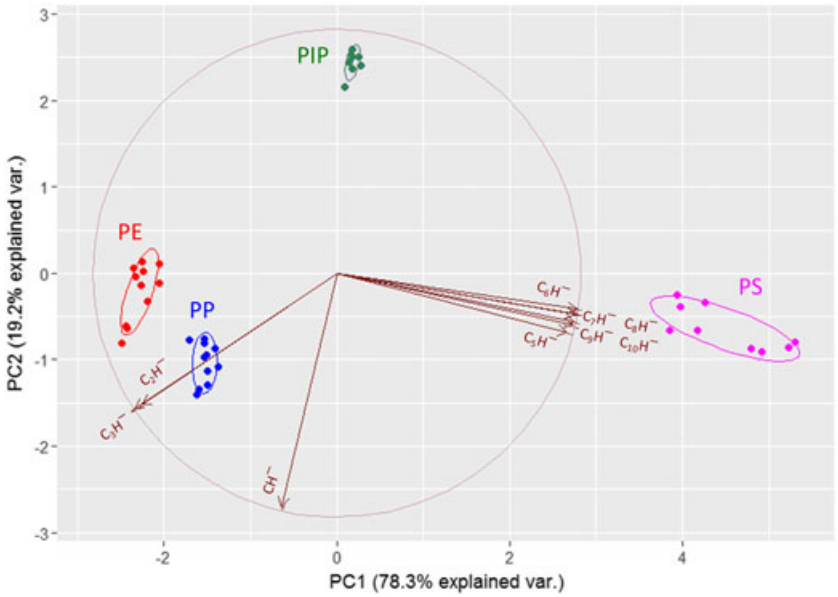

Figure 7. Biplot of scores (points) of observations and loadings (arrowed lines) of variables on PC1 and PC2 from the data normalized by C_4H^- intensity. The 68% data ellipse are shown for scores grouped according to the 4 polymers of polyethylene (PE), polypropylene (PP), polyisoprene (PIP), and polystyrene (PS). Also shown is the correlation circle. The loadings of C_nH^- (excluding C_4H^-) on each of the 2 PCs are multiplied by the square root of their corresponding eigenvalues and scaled along with the radius of the correlation circle.

(Figure 5). Especially, the 2 separated groups within the scores of both PE and PIP as seen in Figure 5 are now closely positioned in Figure 7. The separation between the scores of PE and PP in Figure 7 is more distinctive than that depicted in Figure 5. These observations imply that the normalization by C_4H^- must have removed some contributions irrelevant to the chemical structures of the polymers. It is thus clear that the intensity ratios of C_nH^- to that of C_4H^- are more relevant to the chemical structures of the polymers than their ratios to the total ion intensity.

From both Figures 5 and 7, one can see that the scores of the 4 polymers on PC1 line in the order led by PS and followed by PPI, PP, and PE, with those of PS being at the front of the variable vectors of C_6H^- to $C_{10}H^-$, which is the order of decreasing ρ. Therefore, one can see that PC1 captures what ρ presents, that is, the "carbon density" of the polymers. Our PCA results described above thus echo our argument that higher "carbon density" polymers, such as PS, favor the generation of larger $C_{2n}H^-$ cluster such as C_8H^- and $C_{10}H^-$, while lower "carbon density" polymers such as PE and PP favor the generation of C_2H^- and C_3H^-.[26] We also found that PIP, a polymer with a medium "carbon density," does not affect as much by both the smaller and larger $C_{2n}H^-$. Therefore, it is the "carbon density" of polymers that impacts relationships among the C_nH^- intensities, which is captured by PC1.

Conclusions

We have reviewed our method for delivering OPA SAMs on a hydrophilic surface by either spin or dip coating based on harnessing the unique interaction between OPA molecules and solvents having a dielectric constant ranging from 3 to 5. Solvents meet this requirement include trichloroethylene, chloroform, and anisole. Such a solvent forces the hydrophilic OPA headgroups to the medium surface, allowing delivery of an OPA monolayer on a hydrophilic substrate upon physical contact between it and the medium. We stress that this coating approach is easily scaled-up for industry applications, which can be readily incorporated into a product line for products where surface engineering adds value. The TOF-SIMS has been used to investigate the surface chemistry and chemical stability of OPA SAMs on silicon and aluminum oxides. We have determined that whether OPA molecules are attached to a surface through hydrogen-bonding or covalent bonds can be differentiated by (1) the presence or absence of condensed dimmers ($C_{36}H_{77}P_2O_5^+$ and $C_{36}H_{75}P_2O_5^-$) and (2) abundant or minimal PO_3H^-. The chemical stability of OPA SAMs prepared on the surface of aluminum oxide is limited by oxidation of their hydrocarbon chains starting at approximately 200°C.

We also reviewed our recent work towards development of quantitative analytical approaches to differentiate the chemical structures of polymers. We have found that the ion intensity ratio between C_6H^- and C_4H^-, ρ, provides information pertinent to the chemical structures of PE, PP, PIP, and PS, as well as serves to quantify cross-linking degrees of PMMA films. To understand the relationships among the ion intensities of C_nH^- within the 4 polymers PE, PP, PIP, and PS, we applied the dimensionality reduction technique PCA to analyze C_nH^- (n = 1 to 10) intensity data obtained from the polymers. We demonstrated that biplots, the overlay of the scores of ion intensities and the loadings of C_nH^- on 2 PCs, are an excellent analytical approach to explore the relationships among the ion intensities measured from the polymer samples. By comparing the PCA results from the data set normalized by total ion intensity and that by C_4H^- intensity, we verified that taking ion intensity ratios is indeed a process of removing uncertainties irrelevant to the chemical structure of polymer films. Assisted by the PCA results, we confirmed that lower and higher "carbon density" polymers favor the formation of smaller (eg, C_2H^- and C_3H^-) and larger (ie, C_6H^- to $C_{10}H^-$) C_nH^-, respectively. Moreover, we found that the variability of the C_4H^- intensity against different polymers is relatively small in comparison with other C_nH^- intensities. These experimental findings support the rationale of using ρ to differentiate the chemical structures of polymers, as well as quantifying the cross-linking degrees of PMMA films.

Acknowledgements

The author is thankful for continuous support from Surface Science Western and grateful to collaborators who contributed to the work reviewed in this article: N. Stewart McIntyre, Mary Jane Walzak, James Francis, Woon-Ming Lau, Jieming Feng, Yiliang Wu, Donghan Chen, Yining Huang, and Soheila Naderi-Gohar.

References

[1] A. Ulman, *Chem. Rev.*, **1996**, *96*, 1533–1554.
[2] J. C. Love, L. A. Estroff, J. K. Kriebel, R. G. Nuzzo, G. M. Whitesides, *Chem. Rev.*, **2005**, *105*, 1103–1170.
[3] K. Haupt, K. Mosbach, *Chem. Rev.*, **2000**, *100*, 2495–2504.
[4] D. T. W. Toolan, J. R. Howse, *J. Mater. Chem. C*, **2013**, *1*, 603–616.
[5] H. Ma, H. L. Yip, F. Huang, A. K. Y. Jen, *Adv. Funct. Mater.*, **2010**, *20*, 1371–1388.
[6] H. Klauk, *Chem. Soc. Rev.*, **2010**, *39*, 2643–2666.
[7] K. Norrman, A. Ghanbari-Siahkali, N. B. Larsen, *Annu. Rep. Prog. Chem., Sect. C*, **2005**, *101*, 174–201.
[8] J. M. Spruell, M. Wolffs, F. A. Leibfarth, B. C. Stahl, J. H. Heo, L. A. Connal, J. Hu, C. J. Hawker, *J. Am. Chem. Soc.*, **2011**, *133*, 16698–16706.
[9] S. Edmondson, V. L. Osborne, W. T. S. Huck, *Chem. Soc. Rev.*, **2004**, *33*, 14–22.
[10] C. Hirschl, M. Biebl-ydlo, M. DeBiasio, W. Mühleisen, L. Neumaier, W. Scherf, G. Oreski, G. Eder, B. Chernev, W. Schwab, M. Kraft, *Solar Energy Mater. Solar Cells*, **2013**, *116*, 203–218.
[11] Z. H. Nie, E. Kumacheva, *Nat. Mater.*, **2008**, *7*, 277–290.
[12] S. R. Forrest, *Nature*, **2004**, *428*, 911–918.
[13] C. W. Frank, V. Rao, M. M. Despotopoulou, R. F. W. Pease, W. D. Hinsberg, R. D. Miller, J. F. Rabolt, *Science*, **1996**, *273*, 912–915.
[14] A. Benninghoven, *Angew. Chem. Int. Ed. Engl.*, **1994**, *33*, 1023–1043.
[15] J. S. Fletcher, N. P. Lockyer, S. Vaidyanathan, J. C. Vickerman, *Anal. Chem.*, **2007**, *79*, 2199–2206.
[16] J. C. Vickerman, N. Winograd, *Int. J. Mass Spectrom.*, **2015**, *377*, 568–579.
[17] A. Chilkoti, G. P. Lopez, B. D. Ratner, M. J. Hearn, D. Briggs, *Macromolecules*, **1993**, *26*, 4825–4832.
[18] H.-Y. Nie, *Anal. Chem.*, **2010**, *82*, 3371–3376.
[19] E. A. Jones, N. P. Lockyer, J. C. Vickerman, *Int. J. Mass Spectrom.*, **2007**, *260*, 146–157.
[20] J. Cheng, A. Wucher, N. Winograd, *J. Phys. Chem. B*, **2006**, *110*, 8329–8336.
[21] A. G. Shard, P. J. Brewer, F. M. Green, I. S. Gilmore, *Surf. Interface Anal.*, **2007**, *39*, 294–298.
[22] L. L. Zheng, A. Wucher, N. Winograd, *Anal. Chem.*, **2008**, *80*, 7363–7371.
[23] A. V. Walker, *Anal. Chem.*, **2008**, *80*, 8865–8870.
[24] R. N. S. Sodhi, *Analyst*, **2004**, *129*, 483–487.
[25] A. G. Shard, S. J. Spencer, S. A. Smith, R. Havelund, I. S. Gilmore, *Internat. J. Mass Spectrom.*, **2015**, *377*, 599–609.
[26] H.-Y. Nie, *J. Vac. Sci. Technol. B*, **2016**, *34*, 030603.
[27] S. Naderi-Gohar, K. M. H. Huang, Y. L. Wu, W. M. Lau, H.-Y. Nie, *Rapid Comm. Mass Spectrom.*, **2017**, *31*, 381–388.
[28] I. T. Jolliffe, J. Cadima, *Phil. Trans. R. Soc. A*, **2016**, *374*, 20150202.
[29] D. J. Graham, B. D. Ratner, *Langmuir*, **2002**, *18*, 5861.
[30] X. Vanden Eynde, P. Bertrand, *Surf. Interface Anal.*, **1997**, *25*, 878–888.
[31] G. Coullerez, S. Lundmark, E. Malmstrom, A. Hult, H. J. Mathieu, *Surf. Interface Anal.*, **2003**, *35*, 693–708.
[32] M. L. Pacholski, *Appl. Surf. Sci.*, **2004**, *231-232*, 235–239.
[33] S. Ligot, E. Bousser, D. Cossement, J. Klemberg-Sapieha, P. Viville, P. Dubois, R. Snyders, *Plasma Processes Polym.*, **2015**, *12*, 508–518.
[34] A. L. Hook, D. J. Scurr, *Surf. Interface Anal.*, **2016**, *48*, 226–236.
[35] D. Torres-Salinas, N. Robinson-García, E. Jiménez-Contreras, F. Herrera, E. D. López-Cózar, *J. Am. Soc. Info. Sci. Technol.*, **2013**, *64*, 1468–1479.
[36] H.-Y. Nie, M. J. Walzak, N. S. McIntyre, *Langmuir*, **2002**, *18*, 2955–2958.
[37] H.-Y. Nie, D. J. Miller, J. T. Francis, M. J. Walzak, N. S. McIntyre, *Langmuir*, **2005**, *21*, 2773–2778.
[38] N. S. McIntyre, H.-Y. Nie, A. P. Grosvenor, R. D. Davidson, D. Briggs, *Surf. Interf. Anal.*, **2005**, *37*, 749–754.
[39] H.-Y. Nie, M. J. Walzak, N. S. McIntyre, *J. Phys. Chem. B*, **2006**, *110*, 21101–21108.
[40] J. T. Francis, H.-Y. Nie, N. S. McIntyre, D. Briggs, *Langmuir*, **2006**, *22*, 9244–9250.
[41] H.-Y. Nie, M. J. Walzak, N. S. McIntyre, *ATB Metallurgie*, **2006**, *45*, 564–568.
[42] H.-Y. Nie, N. S. McIntyre, W. M. Lau, *J. Phys.: Conf. Series*, **2007**, *61*, 869–873.
[43] H.-Y. Nie, N. S. McIntyre, W. M. Lau, *Appl. Phys. Lett.*, **2007**, *90*, 203114.
[44] H.-Y. Nie, N. S. McIntyre, W. M. Lau, J. M. Feng, *Thin Solid Films*, **2008**, *517*, 814–818.
[45] H.-Y. Nie, *Anal. Methods*, **2013**, *5*, 4911–4920.
[46] D. H. Chen, H. K.-Y. Wu, S. Naderi-Gohar, Y. L. Wu, Y. N. Huang, H.-Y. Nie, J. Mater, *Chem. C*, **2014**, *2*, 9941–9948.
[47] C. Queffelec, M. Petit, P. Janvier, D. A. Knight, B. Bujoli, *Chem. Rev.*, **2012**, *112*, 3777–3807.
[48] G. Guerrero, J. G. Alauzun, M. Granier, D. Laurencin, P. H. Mutin, *Dalton Trans.*, **2013**, *42*, 12569–12585.
[49] R. C. Longo, K. J. Cho, W. G. Schmidt, Y. J. Chabal, P. Thissen, *Adv. Funct. Mater.*, **2013**, *23*, 3471–3477.
[50] A. Bora, A. Pathak, K.-C. Liao, M. I. Vexler, A. Kuligk, A. Cattani-Scholz, B. Meinerzhagen, G. Abstreiter, J. Schwartz, M. Tornow, *Appl. Phys. Lett.*, **2013**, 241602.
[51] Y. Ito, A. A. Virkar, S. Mannsfeld, J. H. Oh, M. Toney, J. Locklin, Z. N. Bao, *J. Am. Chem. Soc.*, **2009**, *131*, 9396–9404.
[52] U. Zschieschang, T. Yamamoto, K. Takimiya, H. Kuwabara, M. Ikeda, T. Sekitani, T. Someya, H. Klauk, *Adv. Mater.*, **2011**, *23*, 654–658.
[53] B. M. Dhar, R. Özgün, T. Dawidczyk, A. Andreou, H. E. Katz, *Mater. Sci. Eng. R*, **2011**, *72*, 49–80.
[54] O. Acton, M. Dubey, T. Weidner, K. M. O'Malley, T.-W. Kim, G. G. Ting, D. Hutchins, J. E. Baio, T. C. Lovejoy, A. H. Gage, D. G. Castner, H. Ma, A. K.-Y. Jen, *Adv. Funct. Mater.*, **2011**, *21*, 1476–1488.
[55] O. Acton, D. Hutchins, L. Árnadóttir, T. Weidner, N. Cernetic, G. G. Ting, T.-W. Kim, D. G. Castner, H. Ma, A. K.-Y. Jen, *Adv. Mater.*, **2011**, *23*, 1899–1902.
[56] S. P. Pujari, L. Scheres, A. T. M. Marcelis, H. Zuilhof, *Angew. Chem. Int. Ed.*, **2014**, *53*, 6322–6356.
[57] F. S. M. Hashemi, C. Prasittichai, S. F. Bent, *J. Phys. Chem. C*, **2014**, *118*, 10957–10962.
[58] J. A. Zasadzinski, R. Viswanathan, L. Madsen, J. Garnaes, D. K. Schwartz, *Science*, **1994**, *263*, 1726–1733.
[59] R. G. Nuzzo, D. L. Allara, *J. Am. Chem. Soc.*, **1983**, *105*, 4481–4483.
[60] G. M. Whitesides, J. P. Mathias, C. T. Seto, *Science*, **1991**, *254*, 1312–1319.
[61] R. Maoz, J. Sagiv, *J. Colloid Interface Sci.*, **1984**, *100*, 465–496.
[62] J. Gun, R. Iscovici, J. Sagiv, *J. Colloid Interface Sci.*, **1984**, *101*, 201–213.
[63] D. K. Schwartz, *Annu. Rev. Phys. Chem.*, **2001**, *52*, 107–137.
[64] D. Falconnet, G. Csucs, H. M. Grandin, M. Textor, *Biomaterials*, **2006**, *27*, 3044–3063.
[65] J. T. Woodward, A. Ulman, D. K. Schwartz, *Langmuir*, **1996**, *12*, 3626–3629.
[66] B. R. A. Neves, M. E. Salmon, P. E. Russell, E. B. Troughton Jr., *Langmuir*, **2000**, *16*, 2409–2412.
[67] W. Gao, L. Dickinson, C. Grozinger, F. G. Morin, L. Reven, *Langmuir*, **1996**, *12*, 6429–6435.
[68] I. L. Liakos, R. C. Newman, E. McAlpine, M. R. Alexander, *Surf. Interface Anal.*, **2004**, *36*, 347–354.
[69] E. L. Hanson, J. Schwartz, B. Nickel, N. Koch, M. F. Danisman, *J. Am. Chem. Soc.*, **2003**, *125*, 16074–16080.
[70] M. J. Pellerite, T. D. Dunbar, L. D. Boardman, E. J. Wood, *J. Phys. Chem. B*, **2003**, *107*, 11726–11736.
[71] A. Berman, S. Steinberg, S. Campbell, A. Ulman, J. Israelachvili, *Tribol. Lett.*, **1998**, *4*, 43–48.
[72] R. D. Ramsier, P. N. Henriksen, A. N. Gent, *Surf. Sci.*, **1988**, *203*, 72–88.
[73] G. Horowitz, *Adv. Mater.*, **1998**, *10*, 365–377.
[74] H. Sirringhaus, *Adv. Mater.*, **2005**, *17*, 2411–2425.
[75] J. H. Wandass, J. A. Gardella, *J. Am. Chem. Soc.*, **1985**, *107*, 6192–6195.
[76] S. C. C. Wong, N. P. Lockyer, J. C. Vickerman, *Surf. Interface Anal.*, **2005**, *37*, 721–730.
[77] S. Sohn, M. Schroder, D. Lipinsky, H. F. Arlinghaus, *Surf. Interface Anal.*, **2004**, *36*, 1222–1226.
[78] K. V. Wolf, D. A. Cole, S. L. Bernasek, *Anal. Chem.*, **2002**, *74*, 5009–5016.
[79] M. Textor, L. Ruiz, A. Rossi, K. Feldman, G. Hahner, N. D. Spencer, *Langmuir*, **2000**, *16*, 3257–3271.
[80] M. Dubey, T. Weidner, L. J. Gamble, D. G. Castner, *Langmuir*, **2010**, *26*, 14747–14754.
[81] C. Priest, N. Stevens, R. Sedev, W. Skinner, J. Ralston, *J. Colloid Interface Sci.*, **2008**, *320*, 563–568.
[82] K. Niegelhell, S. Leimgruber, T. Grießer, C. Brandl, B. Chernev, R. Schennach, G. Trimmel, S. Spirk, *Langmuir*, **2016**, *32*, 1550–1559.

[83] S. A. Paniagua, A. J. Giordano, O. L. Smith, S. Barlow, H. Li, N. R. Armstrong, J. E. Pemberton, J.-L. Brédas, D. Ginger, S. R. Marder, *Chem. Rev.*, **2016**, *116*, 7117–7158.
[84] H.-Y. Nie, M. J. Walzak, B. Berno, N. S. McIntyre, *Appl. Surf. Sci.*, **1999**, *144-145*, 627–632.
[85] D. Briggs, Surface analysis of polymers by XPS and static SIMS, Cambridge University Press, **1988**, Cambridge, UK.
[86] D. Briggs, *Surf, Interface Anal.*, **1990**, *15*, 734–738.
[87] C.-M. Chan, L.-T. Weng, Y.-T. R. Lau, *Rev. Anal. Chem.*, **2014**, *33*, 11–30.
[88] D. W. Abmayr Jr., *Surf. Sci. Spectra*, **2006**, *13*, 117–165.
[89] T. Trebicky, P. Crewdson, M. Paliy, I. Bello, H.-Y. Nie, Z. Zheng, X. L. Fan, J. Yang, E. R. Gillies, C. Y. Tang, H. Liu, K. W. Wong, W. M. Lau, *Green Chem.*, **2014**, *16*, 1316–1325.
[90] https://www.r-project.org/
[91] https://github.com/vqv/ggbiplot/blob/experimental/R/ggbiplot.r
[92] K. R. Gabriel, *Biometrika*, **1971**, *58*, 453–467.
[93] D. Heller, R. ter Veen, B. Hagenhoff, C. Engelhard, *Surf. Interface Anal.* **2017** (in press, DOI: https://doi.org/10.1002/sia.6269).

